# Maximum usable thickness revisited: Imaging dislocations in Si by modern high-voltage scanning transmission electron microscopy

Sato, Kazuhisa
Research Center for Ultra-High Voltage Electron Microscopy, Osaka University

Yamashita, Yuki
Division of Materials and Manufacturing Science, Graduate School of Engineering, Osaka University

Yasuda, Hidehiro
Research Center for Ultra-High Voltage Electron Microscopy, Osaka University

Mori, Hirotaro
Research Center for Ultra-High Voltage Electron Microscopy, Osaka University



出版情報：Japanese Journal of Applied Physics. 56 (10), pp.100304-, 2017-09-11. 応用物理学会
バージョン：

# Maximum usable thickness revisited: Imaging dislocations in Si by modern high-voltage scanning transmission electron microscopy

Kazuhisa Sato[1, 2*], Yuki Yamashita[2], Hidehiro Yasuda[1, 2], and Hirotaro Mori[1]

[1]Research Center for Ultra-High Voltage Electron Microscopy, Osaka University, Ibaraki, Osaka 567-0047, Japan

[2]Division of Materials and Manufacturing Science, Graduate School of Engineering, Osaka University, Suita, Osaka 565-0871, Japan

*E-mail: sato@uhvem.osaka-u.ac.jp

We have quantitatively evaluated the usable thickness of specimens in scanning transmission electron microscopy (STEM) at 1 MV using a wedge-shaped Si(110) single crystal including artificially introduced high-density dislocations. The width of dislocation images was employed as a criterion for the quantitative evaluation of usable thickness. Superior usable thickness in STEM than in TEM was found; the obtained results were 14.7 μm for STEM and 5.8 μm for TEM. In particular, in STEM, dislocations can be observed as thin lines with 10–15 nm width in the thickness range up to 10 μm. The latest high-voltage STEM is useful for imaging crystal defects in thick semiconductors.

Transmission electron microscopy (TEM) is a powerful technique to analyze materials' microstructures including crystal defects, which determine the strength of metallic materials and the electric properties of semiconductors. For the former, the importance of observing samples of sufficient thickness to be regarded as bulk was proved 50 years ago by using ultrahigh-voltage electron microscopy (UHVEM)[1]. UHVEM developed markedly in the 1970s, and in that era considerable attention was paid to investigating the maximum usable thickness of materials[2-6]. However, the penetration of relativistic electrons depends on observation conditions and materials[7], and quantitative unified conclusions have not been obtained. Recent interest in dislocations formed in compound semiconductors has drawn renewed attention to X-ray topography as well as UHVEM. Although the former technique covers a wide field of view on the millimeter scale, the resolution is limited to μm order[8]. UHVEM is hence the only technique that can reveal the microstructures of a thick sample with μm-order thickness with a high spatial resolution in a multiscale field of view.

In UHVEM observation using a parallel electron beam, chromatic aberration arising from the imaging lens seriously degrades the resolution when observing a thick specimen. Here, the use of an energy filter (EF) to remove inelastic scattering electrons from TEM imaging is an effective solution[9]. On the other hand, scanning transmission electron microscopy (STEM) has the benefit of basically being free from the effect of chromatic aberration; there is no imaging lens for electrons transmitted through a specimen. Moreover, the technique is less affected by the diffraction contrast such as the thickness contour or bend contour owing to the nature of imaging using a converged beam[10]. Hence, STEM can be a suitable technique to observe an extremely thick specimen over 10 μm in thickness. However, there are no reports on STEM

imaging under high voltages regarding the usable thickness and hence this remains an open question.

We hence quantitatively investigate the maximum usable thickness in STEM at 1 MV using a wedge-shaped Si crystal with high-density dislocations introduced artificially as markers. However, the term “usable thickness” is subjective and some clear definition is necessary. In this study, as a standard of usable thickness, we used the theoretical width of dislocation images, which can be defined as $\xi_{hkl} / \pi$, where $\xi_{hkl}$ stands for the extinction distance of the hkl reflection excited for imaging dislocations[11]. Namely, the specimen thickness under which the dislocation line width becomes less than $\xi_{hkl} / \pi$ is thus defined as the maximum usable thickness.

High-density dislocations were introduced into single-crystal Si(110) wafers via indentation using a Vickers hardness tester (Shimadzu HMV-G20, load: 2 kg, dwell time: 2 s) followed by annealing for 600 s at 1123 K in a high-vacuum furnace ($1\times10^{-5}$ Pa). This technique is effective for generating dislocations in silicon wafers as previously reported[12]. Wedge-shaped specimens were cut from the annealed wafers using a focused ion beam (FIB) machine (Hitachi FB-2000A) to identify and select an area of interest near the indentation. The shapes of the prepared wedge-shaped specimens were characterized using a scanning electron microscope (SEM) operating at 10 kV equipped with a cold field emission gun (Hitachi S-5200).

Microstructures of the wedge-shaped specimens including dislocations were characterized by a JEOL JEM-1000EES operating at 1 MV equipped with a $LaB_6$ cathode. We subjected a specimen to a two-beam condition by exciting the 220 reflection of Si. We followed a standard procedure for observing dislocation images since the theory of dislocation image formation based on diffraction contrast has been established[13]. In addition, the invisibility criterion of

dislocations for conventional TEM is also applicable to STEM[14]. Bright-field (BF) TEM images were obtained at a dose rate of $2.7\times10^{22}$ e/m$^2$s using a 20 μm objective aperture with a semiangle of 2.8 mrad. BF-TEM images were recorded using a 2k × 2k charge-coupled device (CCD) camera (Gatan Orius SC200D) with an exposure time of 1-60 s. In the BF-STEM imaging, the beam convergence was set to a semiangle of 3.75 mrad using a 50 μm condenser aperture and the outer collection angle on the BF detector was set to 13 mrad. We used a 200-μm-thick P-43 phosphor scintillator for a BF-STEM detector. STEM images 1k × 1k in size were acquired with a dwell time of 256–1365 μs/pixel depending on the specimen thickness. Under the present observation conditions, primary knock-on damage can occur, while heavy radiation damage such as the amorphization of Si is ruled out[15].

Figure 1(a) shows a secondary electron (SE) image of a wedge-shaped Si crystal viewed in an oblique direction. As can be seen, a triangular cross section is formed, which is suitable for systematically investigating the usable thickness. A schematic illustration of the specimen fixed to a copper grid is shown in Fig. 1(b). Electrons are incident on the crystal from the direction indicated by the arrow. Figure 1(c) summarizes the relationship between the specimen thickness and the horizontal distance measured from the SEM cross-sectional image.

Figure 2 shows a representative BF-STEM image of the wedge-shaped Si shown in Fig. 1(b). The inset at the top left shows a selected area electron diffraction (SAED) pattern satisfying a two-beam condition. The specimen becomes thicker from the left to the right of the image. Dislocations are seen as lines with dark contrast in a bright background. A notable feature is that dislocations can be seen even in the thick region with thickness over 10 μm as marked by arrows. The contrast of the images was adjusted locally in order to show the

dislocations clearly.

Figure 3(a) shows the thickness dependence of the width of the dislocation images measured from TEM and STEM images. The width is defined as full width at half maximum of the image intensity profile measured perpendicular to a dislocation line. The dashed line indicates the criterion $\xi_{220} / \pi = 41$ nm ($\xi_{220} = 130$ nm at 1 MV for Si), and hence data points below this line can be judged to be "observable". As seen, the dislocation width increases as the thickness increases. The obtained maximum usable thickness is 14.7 μm for STEM and 5.8 μm for TEM. The difference in the thickness dependence of the dislocation width in STEM and TEM suggests that the range in which the reciprocity theorem holds is limited. We also found that sharp dislocation images became blurred when observing them from the back side; this can be explained on the basis of the top-bottom effect[16-19]. It was found that the width of dislocation images is independent of collection semiangle of the BF-STEM detector in the range of 4–25 mrad.

Focusing on the results of STEM, the width of dislocation images is 10–15 nm in the thickness range up to 10 μm. This result may be related to the depth of focus of STEM. Figure 3(b) illustrates the STEM probe with convergence semiangle $\alpha$, length of the base of the isosceles triangle $d$, and depth of focus $\Delta z$. When $d$ is equal to the dislocation width $w$, the depth of focus can be approximated as $\Delta z = w / \alpha$. Assigning the values of $w_{max} = 41$ nm and $\alpha = 3.75$ mrad, $\Delta z = 10.9$ μm is obtained. Thus, if we allow the broadening of the width of dislocation images up to 41 nm, an entire 10-μm-thick specimen can be observed in focus using 1 MV STEM. By contrast, assuming the smallest converged probe (approximately 1 nm at 1 MV), a depth of focus as short as 110 nm is derived from $\Delta z = 1.77\lambda / \alpha^2$, where $\lambda$ denotes the

wavelength of incident electrons[20, 21]. As the thickness increases to over 10 μm, the distribution of the dislocation width spreads rapidly. This is presumed to be due to the aforementioned depth of focus as well as the spatial distribution of dislocations. Also note that the detection efficiency of high-voltage STEM depends on the detector performance[22].

Figure 4(a) shows a representative BF-STEM image of a region where dislocations are observed with a line width of about 15 nm. The observed area becomes thicker from the top (6.5 μm) to the bottom (8.5 μm) of the image. Dislocations are seen as dark contrast and the intensity profile shows a valley, as shown in Fig. 4(b), which was obtained from the dislocation marked by a square in Fig. 4(a).

Figure 5 shows a comparison of the results of this study and the literature. The dashed line indicates the results reported by Thomas and Lacaze using 2.5 MV TEM[6]. They observed stacking faults in Si single crystals as a measure of penetration by exciting $g$(hkl) = 220; the imaging conditions are the same as in the present study. Our TEM result as well as the result obtained by Sadamatsu et al.[9] are below the curve obtained by Thomas and Lacaze. In contrast, our STEM result shows a high usable thickness of 14.7 μm at 1 MV. The main reason for the superior usable thickness in STEM compared with that in TEM may be that the chromatic aberration caused by the imaging lens has no effect in the former. We have also examined the usable thickness with a different $g$-vector since the electron transmittance depends on the crystal orientation[7]; $g$(hkl) = 111 resulted in a degradation of usable thickness (7.5 μm for 1 MV STEM).

In summary, we have demonstrated the superior usable thickness of specimens in STEM than in TEM, both at 1 MV. The maximum usable thickness measured from a wedge-shaped Si

single crystal was 14.7 μm for STEM and 5.8 μm for TEM. The superior usable thickness in STEM may have been caused by the imaging being free from chromatic aberration, as initially expected. High-voltage STEM is thus useful for imaging crystal defects in thick semiconductors of current interest. The maximum usable thickness depends not only on the material but also on the imaging conditions; we have introduced a clear criterion for the quantitative evaluation of usable thickness. The criterion, however, can be changed according to the purposes or targets of observations. The effect of the spatial distribution of dislocations is not considered explicitly here, while it must be clarified in future since it will affect the visibility of dislocations. In order to image a thick specimen having a thickness exceeding μm order, ensuring a sufficient signal strength is mandatory. A more detailed analysis of dislocations in Si and other semiconductors is ongoing.

**Acknowledgments** The authors wish to thank Mr. A. Ohsaki, Mr. Y. Agatsuma, Mr. S. Takakuwa, Dr. S. Ohta, and Mr. M. Ohsaki of JEOL Ltd. for their support using the JEM-1000EES. KS acknowledges Mr. E. Taguchi, Mr. T. Yasuda, and Ms. Y. Hiraizumi of Osaka University for their technical assistance with the FIB, SEM, and TEM, and Dr. K. Asayama of JEOL Ltd. and Dr. J. Yamasaki of Osaka University for invaluable comments. This study was partially supported by JSPS KAKENHI Grant Numbers JP16K13640 and JP17H02746.

1. H. Fujita, Y. Kawasaki, E. Furubayashi, S. Kajiwara, and T. Taoka, Jpn. J. Appl. Phys. **6**, 214 (1967).
2. R. Uyeda and M. Nonomiya, Jpn. J. Appl. Phys. **7**, 200 (1968).
3. K. F. Hale and M. Henderson Brown, Nature **221**, 1232 (1969).
4. H. Fujita, T. Tabata, K. Yoshida, N. Sumida, and S. Katagiri, Jpn. J. Appl. Phys. **11**, 1522 (1972).
5. H. Fujita and T. Tabata, Jpn. J. Appl. Phys. **12**, 471 (1973).
6. G. Thomas and J.-C. Lacaze, J. Microsc. **97**, 301 (1973).
7. C. J. Humphreys, L. E. Thomas, J. S. Lally, and R. M. Fisher, Philos. Mag. **23**, 87 (1971).
8. H. Matsuhata, H. Yamaguchi, and T. Ohno, Philos. Mag. **92**, 4599 (2012).
9. S. Sadamatsu, M. Tanaka, K. Higashida, and S. Matsumura, Ultramicroscopy **162**, 10 (2016).
10. C. J. Humphreys, Ultramicroscopy **7**, 7 (1981).
11. B. Fultz and J. M. Howe, *Transmission Electron Microscopy and Diffractometry of Materials* (Springer, Berlin, 2008), 3rd ed.
12. M. Tanaka, K. Higashida, K. Kaneko, S. Hata, and M. Mitsuhara, Scr. Mater. **59**, 901 (2008).
13. P. Hirsch, A. Howie, R. B. Nicholson, D. W. Pashley, and M. J. Whelan, *Electron Microscopy of Thin Crystals* (Krieger, Malabar, FL, 1977), 2nd ed.
14. P. J. Phillips, M. C. Brandes, M. J. Mills, and M. De Graef, Ultramicroscopy **111**, 1483 (2011).
15. J. Yamasaki, S. Takeda, and K. Tsuda, Phys. Rev. B **65**, 115213 (2002).
16. H. Hashimoto, J. Appl. Phys. **35**, 277 (1964).

17. P. Gentisch, H. Gilde, and L. Reimer, J. Microsc. **100**, 81 (1974).

18. Y. Oshima, R. Nishi, K. Asayama, K. Arakawa, K. Yoshida, T. Sakata, E. Taguchi, and H. Yasuda, Microscopy **62**, 521 (2013).

19. J. Yamasaki, M. Mori, A. Hirata, Y. Hirotsu, and N. Tanaka, Ultramicroscopy **151**, 224 (2015).

20. P. D. Nellist, *Scanning Transmission Electron Microscopy*, ed. S. J. Pennycook and P. D. Nellist (Springer, New York, 2011), Chap.2.

21. T. Kiguchi, Y. Yamaguchi, S. Tashiro, K. Sato, and T. J. Konno, Mater. Trans. **56**, 1633 (2015).

22. A. Ishikawa, C. Morita, M. Hibino, and S. Maruse, J. Electron Microsc. **29**, 341 (1980).

Figure legends

Fig. 1 (a) SE image of a wedge-shaped Si crystal, (b) schematic illustration of the specimen fixed to a copper grid, and (c) relationship between the specimen thickness and the horizontal distance measured from the SEM cross-sectional image.

Fig. 2 Representative BF-STEM image and the corresponding SAED pattern of the wedge-shaped Si. Arrows indicate dislocations. The contrast of the images was adjusted locally in order to show the dislocations clearly.

Fig. 3 (a) Thickness dependence of the width of dislocation images measured from TEM and STEM images. (b) Schematic illustration of converged STEM probe with convergence semiangle $\alpha$, length of the base of the isosceles triangle $d$, and depth of focus $\Delta z$. The dotted line represents the optic axis.

Fig. 4 (a) Representative BF-STEM image of a region where dislocations are observed with a line width of about 15 nm. (b) Intensity profile measured perpendicular to the dislocation marked by a square in (a).

Fig. 5 Comparison of the usable thickness obtained in this study and those reported in the literature. The usable thickness of 1 MV STEM is comparable to that of previous 2.5 MV TEM.

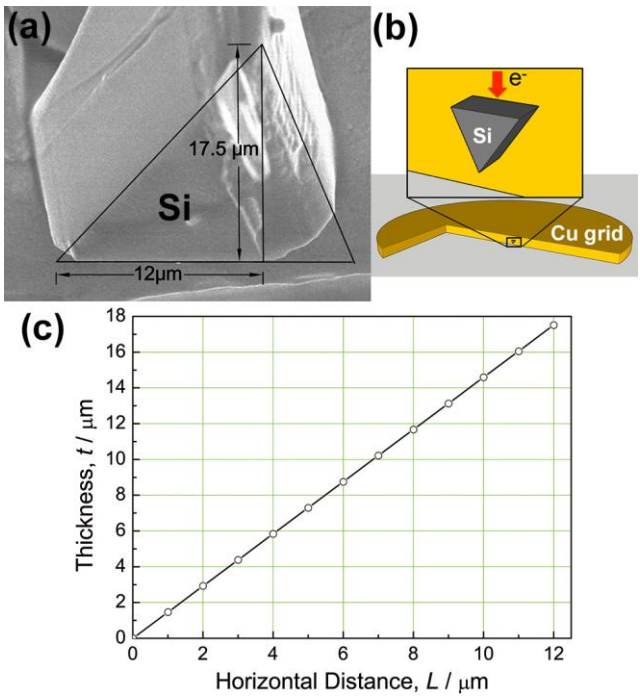


Sato et al. Fig.1

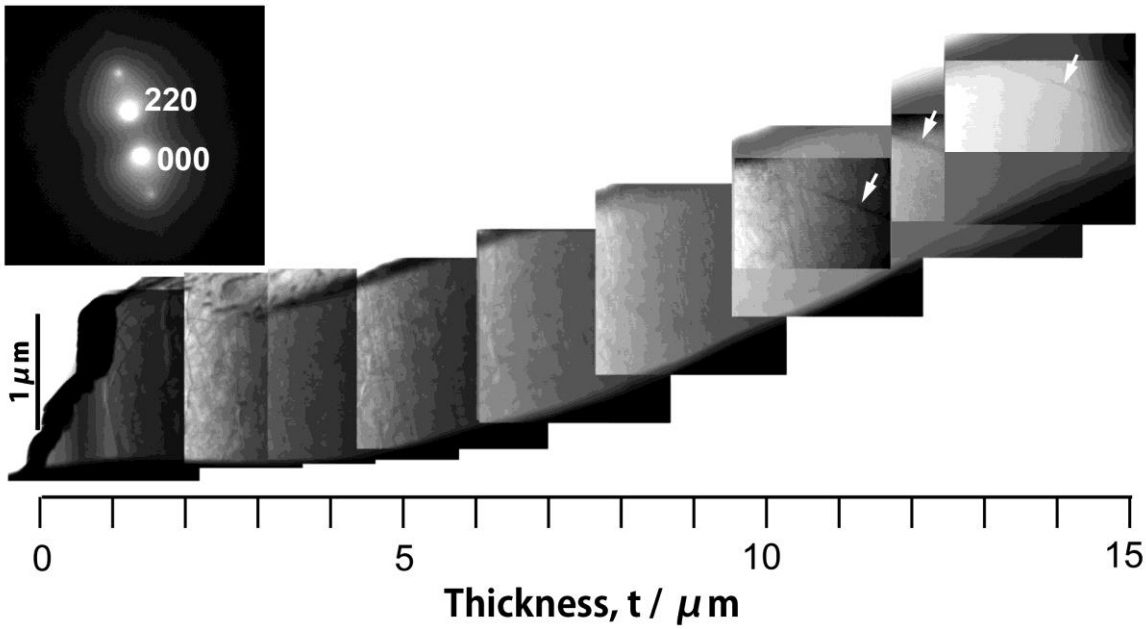


Sato et al. Fig.2

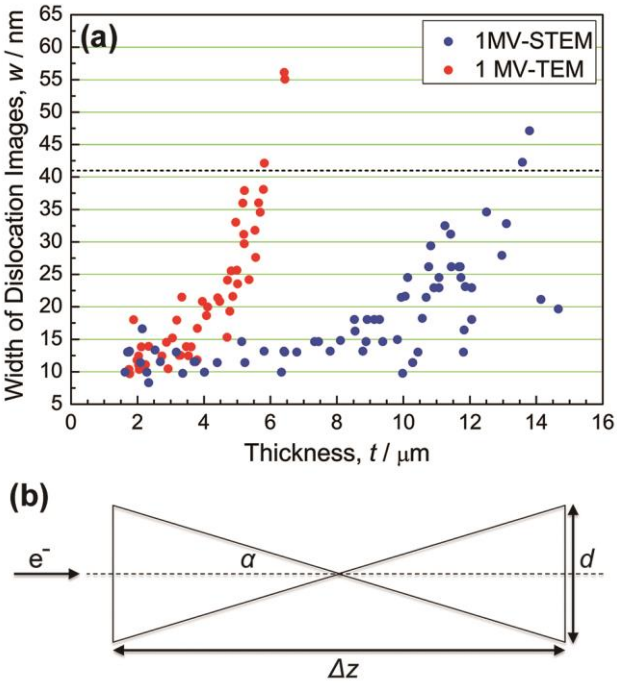


Sato et al. Fig.3

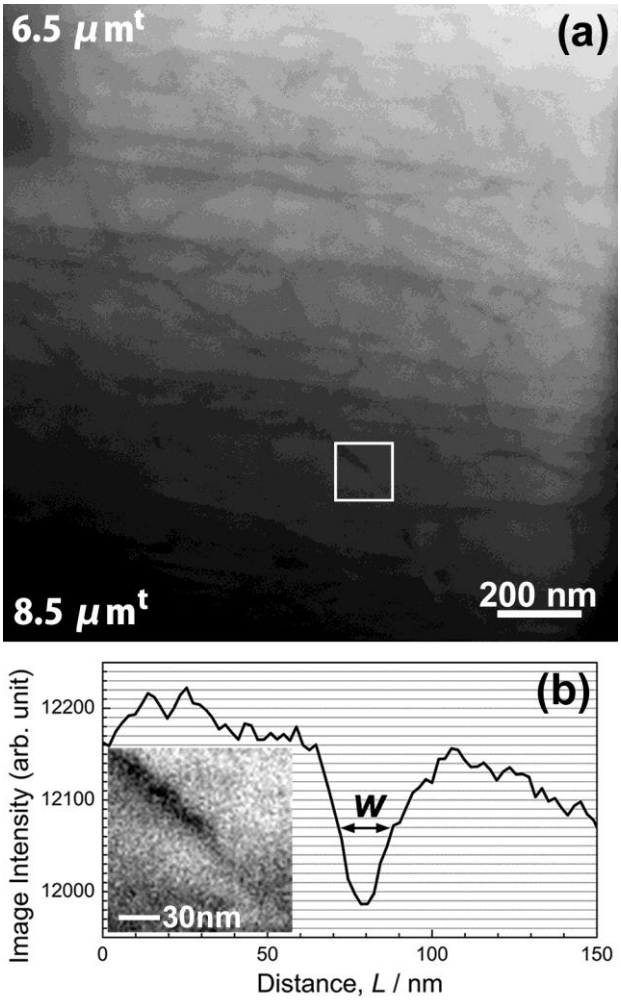


Sato et al. Fig.4

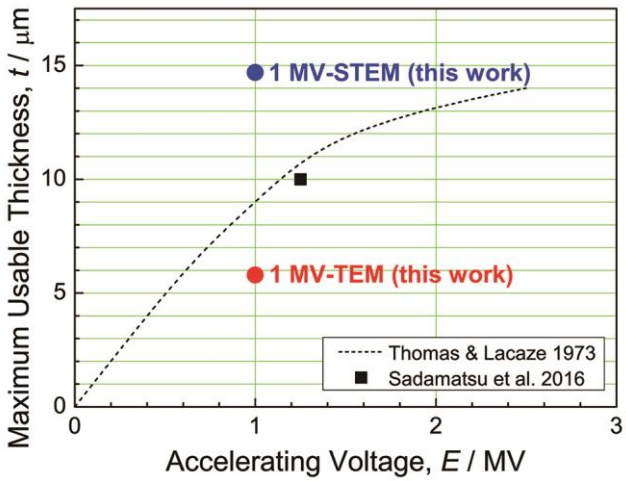


Sato et al. Fig.5